https://doi.org/10.5194/egusphere-2026-1709
Preprint. Discussion started: 8 April 2026

ORACLE-lite (v3.0): A reduced-complexity module for simulating organic aerosol formation and evolution in long term chemistry-climate simulations

Alexandra P. Tsimpidi and Vlassis A. Karydis

Institute of Climate and Energy Systems: Troposphere (ICE-3), Forschungszentrum Jülich GmbH, Jülich, Germany

Correspondence to: Alexandra P. Tsimpidi (a.tsimpidi@fz-juelich.de)

Abstract

The representation of organic aerosol (OA) in global chemistry–climate models remains computationally challenging due to the large number of volatility-resolved tracers required to simulate gas–particle partitioning and aging. We present ORACLE-lite (v3.0), a reduced-complexity version of the ORACLE module implemented within the ECHAM/MESSy Atmospheric Chemistry (EMAC) model, specifically designed for multi-decadal simulations. ORACLE-lite preserves the core mechanisms governing OA formation while employing the minimum number of surrogate tracers required to represent organic compounds across the principal volatility classes, including low-volatility (LVOC), semi-volatile (SVOC), intermediate-volatility (IVOC), and volatile organic compounds (VOC). This structured reduction lowers the computational cost per model time step by a statistically robust speed-up of 13.9 ± 1.1%, enabling efficient multi-decadal simulations while maintaining a dynamic representation of volatility evolution. ORACLE-lite is evaluated in a 21-year global simulation (2000–2020) and compared against the standard ORACLE configuration. The simplified volatility basis set modifies gas–particle partitioning, leading to enhanced primary organic aerosol (POA) concentrations of up to 5 μg m^{-3} over major biomass-burning and industrial regions, while secondary organic aerosol (SOA) concentrations decrease over biomass-burning regions and increase over anthropogenic source regions due to differences in precursor allocation among volatility bins. Model performance is assessed against long-term aerosol mass spectrometer (AMS) and aerosol chemical speciation monitor (ACSM) observations across North America, Europe, and Eastern Asia. Simulated total OA agrees well with observations over North America (normalized mean bias, NMB = −4%) and Eastern Asia (NMB = −29%), while larger seasonal biases occur in Europe, particularly in winter. Over tropical and subtropical regions, the model shows an overall underestimation (NMB ≈ −39%) with substantial regional variability. Across all regions, the model reproduces the observed spatial distribution and seasonal variability of OA mass and its primary and secondary components within a factor of two for the majority of sites. These results demonstrate that ORACLE-lite provides a computationally efficient and physically grounded framework capable of reproducing the key features of global OA variability, making it suitable for long-term chemistry–climate simulations.

https://doi.org/10.5194/egusphere-2026-1709
Preprint. Discussion started: 8 April 2026

1. Introduction

Organic aerosol (OA) constitutes a significant fraction of atmospheric particulate matter and plays an important role in air quality, human health, and climate through its influence on radiation, cloud formation, and atmospheric chemistry (Kanakidou et al., 2005; Hallquist et al., 2009; Jimenez et al., 2009). Traditionally, OA has been classified as primary organic aerosol (POA), emitted directly from sources, and secondary organic aerosol (SOA), formed in the atmosphere from the oxidation of volatile organic compounds (VOCs). However, organic emissions span a continuum of effective volatilities, ranging from low-volatility organic compounds (LVOCs) to semivolatile organic compounds (SVOCs), intermediate-volatility organic compounds (IVOCs), and VOCs. Although most organic emissions are initially in the gas phase, multi-generational oxidation can transform high-volatility precursors into lower-volatility products that partition to the particle phase (Donahue et al., 2011). The evolution of this continuum of organic vapors through gas–particle partitioning and multiphase chemistry governs OA composition, volatility, and climate-relevant properties (Hodzic and Jimenez, 2011; Donahue et al., 2012a). Representing these processes in atmospheric models remains challenging, particularly in long-term chemistry–climate simulations, where computational constraints require simplified yet physically based parameterizations (Spracklen et al., 2011; Shrivastava et al., 2017; Riipinen et al., 2026).

Considerable progress has been made through the development of volatility basis set (VBS) frameworks (Donahue et al., 2006; Tsimpidi et al., 2010; Tsimpidi et al., 2011; Murphy et al., 2011; Bergstrom et al., 2012; Tsimpidi et al., 2014, 2018), which provide a physically grounded representation of OA partitioning and aging. Nevertheless, most global and climate-scale models continue to rely on simplified SOA parameterizations (Tsigaridis et al., 2014; Shrivastava et al., 2017; Riipinen et al., 2026). These approaches typically employ fixed SOA yields, limited precursor classes, or single-generation oxidation schemes, which are unable to represent the non-linear response of OA to changes in emissions, oxidant levels, and thermodynamic conditions (Pye et al., 2019; Hodzic et al., 2020). In addition, commonly used “simple SOA” formulations neglect the evolution of volatility, the competition between functionalization and fragmentation, and differences in the aging behavior of biogenic and anthropogenic precursors (Donahue et al., 2012b). As a consequence, such models often underestimate OA variability and struggle to reproduce observed regional patterns and sensitivities to emission perturbations (Hodzic et al., 2016; Pai et al., 2020).

These limitations are particularly relevant under future climate conditions. Projected changes in biogenic VOC emissions, NO_x availability, oxidant concentrations, and wildfire activity are expected to substantially influence OA formation pathways (Peñuelas and Staudt, 2010; Young et al., 2013; Van Der Werf et al., 2017). Increasing temperatures may shift semi-volatile partitioning toward the gas phase, while enhanced oxidation capacity can promote more extensive multi-generational aging and the formation of highly oxygenated and extremely low-volatility organic compounds (Ehn et al., 2014; Bianchi et al., 2019). Such changes affect OA lifetime, hygroscopicity, and radiative effects, highlighting the need for OA schemes in climate models that are both computationally efficient and able to respond dynamically to evolving atmospheric

https://doi.org/10.5194/egusphere-2026-1709
Preprint. Discussion started: 8 April 2026

conditions. However, no existing OA scheme that is suitable for global chemistry–climate models can simultaneously represent multi-generational aging and volatility evolution while remaining computationally feasible for multi-decadal simulations.

The ORACLE model framework has progressively advanced the representation of OA in global chemistry–climate models. The original ORACLE module (Tsimpidi et al., 2014), hereafter referred to as ORACLE-base, was among the first implementations of a VBS approach in a global chemical transport model, enabling a physically based representation of OA composition and evolution. ORACLE-2D (Tsimpidi et al., 2018) extended this framework to a two-dimensional VBS, representing changes in both volatility and oxidant content during atmospheric aging, which influence key climate-relevant properties such as hygroscopicity (Lambe et al., 2011). Subsequent developments coupled ORACLE with a more detailed VOC chemical mechanism, enabling process-oriented studies in short-term and high-resolution simulations (Pozzer et al., 2022). More recently, ORACLE has been expanded to include a lumped IVOC mechanism (ORACLE-IVOC), simulating SOA formation from IVOC emissions using a multi-product approach (Scholz et al., 2025). While these developments have improved process representation and model performance, their computational expense limits their applicability in multi-decadal chemistry–climate simulations.

A first proof-of-concept application of a reduced-complexity ORACLE configuration was performed by Tsimpidi et al. (2025), where a slightly reduced set of OA tracers was employed to enable a 20-year simulation of aerosol composition. That study demonstrated the feasibility of using a simplified volatility-based representation for long-term applications while maintaining physically meaningful OA behavior. Building on this initial exploration, the present study formally introduces ORACLE-lite (v3.0) as a fully documented, standalone, and computationally efficient OA scheme specifically designed for multi-decadal chemistry–climate simulations.

ORACLE-lite preserves the core mechanisms governing OA formation and multi-generational aging while employing the minimum set of surrogate tracers required to represent OA formation from the principal volatility classes (LVOCs, SVOCs, IVOCs, and VOCs). This physically constrained reduction substantially lowers computational cost while maintaining a dynamic representation of volatility evolution, thereby enabling decadal-scale simulations of OA formation and evolution. Here, we describe the development and implementation of ORACLE-lite, quantify its computational efficiency relative to ORACLE-base, and evaluate its performance against long-term aerosol mass spectrometer (AMS/ACSM) observations of OA mass and speciation across multiple regions and environments worldwide. With this, we assess its suitability for multi-decadal simulations of OA composition and evolution in the atmosphere in global chemistry–climate models.

https://doi.org/10.5194/egusphere-2026-1709
Preprint. Discussion started: 8 April 2026

2. Model Description

2.1 The EMAC model

The ECHAM/MESSy Atmospheric Chemistry (EMAC) model is a numerical chemistry–climate simulation system that includes submodels describing lower and middle atmospheric processes and their interactions with the oceans, land, and anthropogenic influences. EMAC consists of the Modular Earth Submodel System (MESSy) (Jöckel et al., 2010) coupled with an advanced version of the fifth-generation European Centre Hamburg (ECHAM5) general circulation model (Roeckner et al., 2006). ECHAM5 serves as the atmospheric dynamical core that simulates atmospheric flow and is integrated into the base-model layer of MESSy (Jöckel et al., 2006). The MESSy interface structure links the base model with several atmospheric submodels that simulate, online, gas-phase chemistry (MECCA) (Sander et al., 2019), inorganic aerosol microphysics and dynamics (GMXe) (Pringle et al., 2010), organic aerosol formation and growth (ORACLE) (Tsimpidi et al., 2014), emissions (ONLEM and OFFLEM) (Kerkweg et al., 2006a), dry deposition and sedimentation (DRYDEP and SEDI) (Kerkweg et al., 2006b), cloud scavenging (SCAV) (Tost et al., 2006), cloud microphysics (CLOUD) (Röckner et al., 2006), and aerosol optical properties (AEROPT) (Lauer et al., 2007). In this study, EMAC is applied at a spectral resolution of T63L31, corresponding to a horizontal grid resolution of 1.875° × 1.875° and 31 vertical layers extending up to 18 km altitude (10 hPa). The model is run for 21 years covering the period 2000–2020, with the first year used as spin-up.

2.2 The ORACLE-base module

ORACLE is a computationally efficient module for describing the composition and evolution of organic aerosol in the atmosphere (Tsimpidi et al., 2014), and it has been incorporated into the EMAC model. Over time, several configurations of ORACLE have been developed to address different scientific objectives and model applications (Figure 1). These include the original ORACLE-base formulation (Tsimpidi et al., 2014), the ORACLE-2D extension that tracks OA evolution in both volatility and oxygenation space (Tsimpidi et al., 2018), the ORACLE-IVOC configuration that represents SOA formation from intermediate-volatility organic compound emissions using a lumped precursor approach (Scholz et al., 2025), and the ORACLE-PRO configuration coupled with an advanced chemical mechanism for process-oriented studies in short-term simulations (Pozzer et al., 2022). Figure 1 summarizes the main developments of the ORACLE family within the EMAC system and their typical simulation timescales and intended modeling applications.

The original version of ORACLE (ORACLE-base) simulates the volatility distribution of a wide variety of semi-volatile organic surrogate compounds using bins of logarithmically spaced effective saturation concentrations. Organic emissions from multiple anthropogenic and natural sources are represented using distinct surrogate species for each source category. These surrogates are grouped according to their volatility to LVOCs ($C^* \leq 10^{-1}$ μg m^{-3}), SVOCs ($10^{-1} < C^* \leq 10^{2}$ μg m^{-3}), IVOCs ($10^{2} < C^* \leq 10^{6}$ μg m^{-3}), and VOCs ($C^* > 10^{6}$ μg m^{-3}). These organic compounds

https://doi.org/10.5194/egusphere-2026-1709
Preprint. Discussion started: 8 April 2026

are allowed to partition between the gas and aerosol phases, resulting in the formation of organic aerosol (OA). Changes in the aerosol mass of each size mode after partitioning are calculated using a weighting factor as described in Tsimpidi et al. (2014). Gas-phase photochemical reactions that alter compound volatility are also included, and the oxidation products of each precursor group are simulated separately to preserve information about their source. Model predictions for the various organic aerosol components have been evaluated using factor-analytic results from a comprehensive set of aerosol mass spectrometer (AMS) measurements collected during multiple field campaigns across the Northern Hemisphere (Tsimpidi et al., 2016). The good agreement between campaign-average concentrations and model predictions demonstrates the ability of ORACLE to capture the spatial and temporal variability of OA.

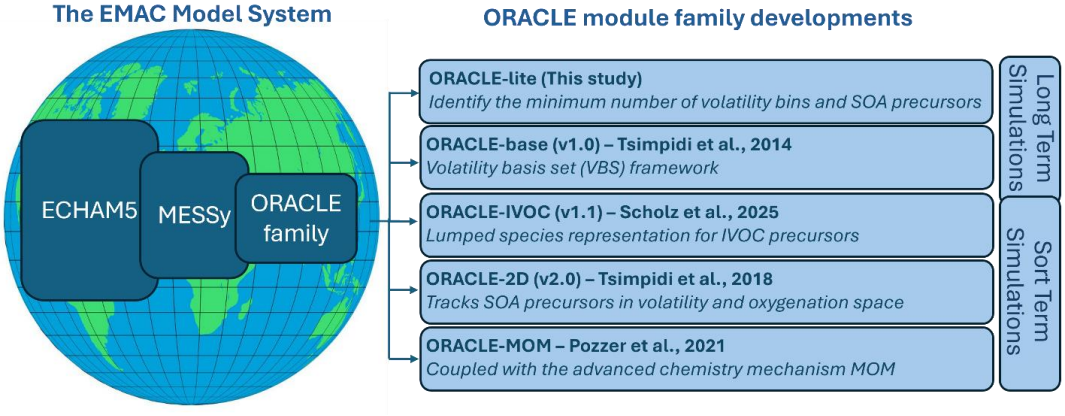

Figure 1: Different versions of the ORACLE module (ORACLE family) implemented in the EMAC model system for short- and long-term model applications.

2.3 The ORACLE-lite module

The lite version proposed here includes three surrogate species for POA with saturation concentrations (C^*) at 298 K equal to 10^{-2}, 10^{1}, and 10^{4} μg m^{-3}. The least volatile fraction, with C^* = 10^{-2} μg m^{-3}, represents low-volatility organics that reside predominantly in the particulate phase, even in remote regions (LVOC). The 10^{1} μg m^{-3} bin describes semivolatile organics that partition between the gas and particle phases under typical atmospheric conditions (SVOC). Finally, even under highly polluted conditions, the majority of material in the 10^{4} μg m^{-3} bin remains almost entirely in the vapor phase (IVOC).

A similar approach is applied to SOA formed from VOCs. In the lite version of ORACLE, the oxidation of anthropogenic and biogenic VOC species produces two oxidation products per precursor, distributed into two volatility bins with effective saturation concentrations at 298 K of 1 and 10^{3} μg m^{-3}. A schematic overview of the ORACLE-lite module, illustrating the different aerosol types and chemical processes represented in the model, is shown in Figure 2.

https://doi.org/10.5194/egusphere-2026-1709
Preprint. Discussion started: 8 April 2026

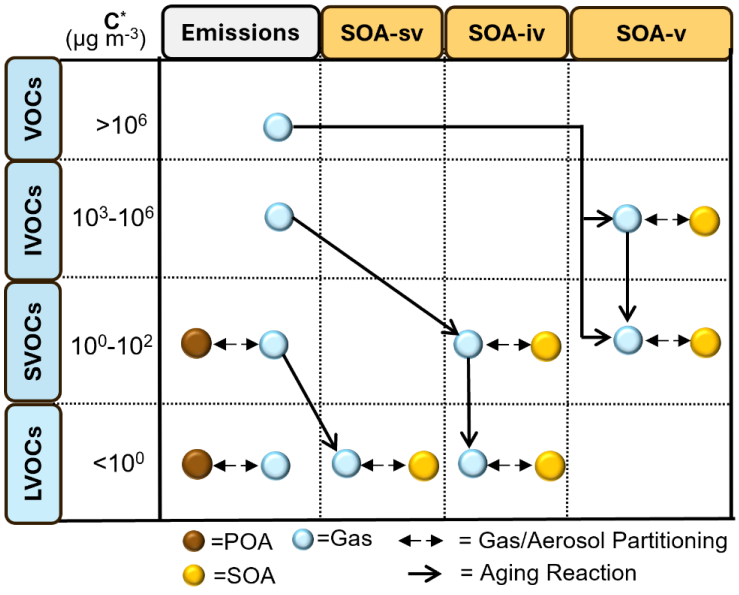

Figure 2: Schematic representation of primary and secondary organic aerosol formation pathways from VOC, IVOC, SVOC, and LVOC emissions in ORACLE-lite.

2.3.1 LVOC/SVOC/IVOC emissions

ORACLE-lite distinguishes organic emissions from biomass burning and other combustion sources (biofuel, fossil fuel combustion, and other urban sources) by applying different emission factors for each category. The module uses the same three surrogate species to represent POA volatility, with effective saturation concentrations at 298 K of C* = 10^{-2}, 10^{1}, and 10^{4} μg m^{-3}, corresponding to LVOCs, SVOCs, and IVOCs. The emission factors that distribute traditional POA emissions among these three volatility bins follow Tsimpidi et al. (2016). For anthropogenic combustion sources (fossil fuel and biofuel combustion), the emission factors are 0.09, 0.71, and 1.7 for LVOC, SVOC, and IVOC, respectively. These factors also account for additional IVOC emissions that are missing from traditional inventories. Here, we assume that missing IVOC emissions from anthropogenic combustion sources are equal to 1.5 times the traditional OA emissions in the inventory; therefore, the sum of the emission factors for anthropogenic sources is 2.5. For open biomass burning, the emission factors are 0.2, 0.5, and 0.3 for LVOC, SVOC, and IVOC, respectively. No additional IVOC emissions are included for open biomass burning, so the sum of the biomass-burning emission factors is unity.

LVOCs and SVOCs are assumed to be emitted as POA, whereas IVOCs are emitted as primary organic gases (POG). These compounds are then allowed to partition between the gas and particle phases. The fraction that remains in the aerosol phase after this initial partitioning is defined as POA, while the fraction in the gas phase is considered POG. The gas-phase material (POG) can subsequently undergo oxidation and form SOA (Figure 2).

https://doi.org/10.5194/egusphere-2026-1709
Preprint. Discussion started: 8 April 2026

2.3.2 Photochemical Reactions

Photo-oxidation of VOCs: The photochemical oxidation of VOCs that serve as SOA precursors is included in the gas-phase chemical mechanism, which includes the oxidation of alkenes, aromatics, and isoprene by OH, as well as the oxidation of olefins and monoterpenes by O_3, O, OH, and NO_3 (Tsimpidi et al., 2014). Oxidation products from anthropogenic VOCs (aVOCs: alkenes, aromatics, and olefins) and from biogenic VOCs (bVOCs: monoterpenes and isoprene) are lumped into two secondary organic gases (SOG-v) distributed into volatility bins with logarithmically spaced effective saturation concentrations at 298 K equal to 10^0 and 10^3 μg m^{-3}. (Figure 2). The formation of SOA from the photo-oxidation of VOC (SOA-v) is represented by the following reactions:

$$\text{VOC} + \text{Oxidants} \rightarrow a_1\,\text{SOG-v}_1 + a_2\,\text{SOG-v}_2 \qquad \text{(R1)}$$

$$\text{SOG-v}_i \leftrightarrow \text{SOA-v}_i \qquad \text{(R2)}$$

where a_i is the aerosol yield for volatility bin i (with i=1,2; Table 1). The lite version includes two volatility bins, and the corresponding aerosol yields are taken from laboratory smog-chamber experiments under high-NO_x conditions for anthropogenic VOCs and low-NO_x conditions for biogenic VOCs (Tsimpidi et al., 2014). This approach assumes that urban areas, where most anthropogenic VOCs are emitted (~90%), are generally characterized by high-NO_x levels (Tsimpidi et al., 2008; Karl et al., 2009), while forested regions are characterized by low-NO_x conditions (Pugh et al., 2010; Browne et al., 2013).

Table 1: Correspondence between ORACLE VOC groups and the CAMS-GLOB emission VOC groups, together with the corresponding volatility-dependent SOA yields. SOA yields are calculated assuming a particle density of 1.5 g cm^{-3}.

ORACLE VOC group	CAMS-GLOB VOC Compound	MW	SOA yield	
		(g/mol)	(C_1*=10^0μg m^{-3})	(C_2*=10^3 μg m^{-3})
ARO1	Benzene / Toluene	100.47	0.168	0.735
ARO2	Xylene/Trimethyl_Benzenes + other aromatics	113.93	1.197	0.735
OLE1	Propene	61.68	0.006	0.188
OLE2	Other alkenes	79.05	0.029	0.353
ALK4	Pentanes	73.23	0.038	0.000
ALK5	hexanes and higher alkanes	106.97	0.150	0.000
C5H8	Isoprene	68.12	0.039	0.015
TERP	Monoterpenes	136.24	0.199	0.959

Chemical Aging Reactions: ORACLE treats all OA compounds as chemically reactive; however, only homogeneous gas-phase aging is included because it proceeds more rapidly than heterogeneous reactions with OH (Donahue et al., 2013). In the lite version, the volatilities of OA surrogate species reacting with OH are reduced by a factor of 10^3 (Figure 2), with a reaction rate constant of 0.33×10^{-11} cm^3 $molecule^{-1}$ s^{-1}, and their mass is increased by 22.5% to account for the

https://doi.org/10.5194/egusphere-2026-1709
Preprint. Discussion started: 8 April 2026

addition of three oxygen atoms, assuming a C_{15} precursor. This represents a more aggressive reduction in volatility and oxygen addition compared with the standard ORACLE version, but with a reduced reaction rate constant. Existing evidence suggests that aging of biogenic SOA does not lead to substantial changes in mass concentration (Ng et al., 2006; Donahue et al., 2012b; Murphy et al., 2012); therefore, their chemical aging is assumed here not to produce a net increase in SOA mass. The chemical aging of SOA is described by the following reactions:

$$\text{aSOG-v}_2 + \text{OH} \rightarrow 1.225\ \text{aSOG-v}_1 \quad \text{(R5)}$$
$$\text{aSOG-v}_1 \leftrightarrow \text{aSOA-v}_1 \quad \text{(R6)}$$
$$\text{SVOC} + \text{OH} \rightarrow 1.225\ \text{SOG-sv} \quad \text{(R7)}$$
$$\text{SOG-sv} \leftrightarrow \text{SOA-sv} \quad \text{(R8)}$$
$$\text{IVOC} + \text{OH} \rightarrow 1.225\ \text{SOG-iv}_2 \quad \text{(R9)}$$
$$\text{SOG-iv}_2 + \text{OH} \rightarrow 1.225\ \text{SOG-iv}_1 \quad \text{(R10)}$$
$$\text{SOG-iv}_i \leftrightarrow \text{SOA-iv}_i \quad \text{(R11)}$$

2.3.3 Gas/Aerosol Partitioning

ORACLE calculates the partitioning of organic compounds between the gas and particle phases by assuming bulk equilibrium and that all organic compounds form a pseudo-ideal solution. The gas–aerosol partitioning is performed in two steps, as described below (Figure 3).

Bulk equilibrium: ORACLE first calculates the bulk equilibrium gas and aerosol phase concentrations following the approach of the SOAM II model of Strader et al. (1999). Considering the partitioning of n organic compounds and assuming a pseudo-ideal solution, a set of n nonlinear equations is obtained:

$$c_{a,i} = c_{t,i} - x_i c_i^* \text{ for } i = 1, n \quad \text{(E1)}$$

$$x_i = \frac{c_{a,i}/M_i}{\sum_{j=1}^{n} c_{a,j}/M_j}, \quad \text{(E2)}$$

where $c_{t,i}$ and $c_{a,i}$ are the total and aerosol-phase concentrations of product i (μg m^{-3}), c_i^* is the effective saturation concentration, x_i is the mole fraction of product i in the absorbing organic phase, and M_i is its the molecular weight. Molecular weights of 250 g mol^{-1} are assumed for all POA, SOA-sv, and SOA-iv components, while bSOA-v and aSOA-v are assigned molecular weights of 180 and 150 g mol^{-1}, respectively (Tsimpidi et al., 2014). The temperature dependence of the saturation concentration is described by the Clausius–Clapeyron equation:

$$c_i^* = c_{i,0}^* \frac{T_0}{T} \exp\left[\frac{\Delta H}{R}\left(\frac{1}{T_0} - \frac{1}{T}\right)\right], \quad \text{(E3)}$$

where c_i^* and $c_{i,0}^*$ are the saturation concentrations at temperatures T and T_0, respectively, R is the gas constant, and ΔH is the enthalpy of vaporization. In this application, an effective ΔH of 30 kJ

https://doi.org/10.5194/egusphere-2026-1709
Preprint. Discussion started: 8 April 2026

mol^{-1} is used for all SOA-v species, based on data for α-pinene (Pathak et al., 2007). Enthalpy values of 112, 94, and 76 kJ mol^{-1} are used for the 10^{-2}, 10^{1}, and 10^{4} µg m^{-3} volatility bins, respectively, for all organic compounds from fuel combustion and biomass burning sources based on data for large saturated species commonly found in primary emissions (Donahue et al., 2006). ORACLE solves this set of equations to determine the bulk aerosol composition at equilibrium.

Aerosol size distribution: The aerosol size distribution is then determined by allocating the change in aerosol mass after bulk equilibrium to each size mode using a weighting factor (Pandis et al., 1993). Assuming a pseudo-ideal solution, the fraction $f_{i,k}$ of the total flux of species i that condenses onto or evaporates from aerosol mode k is given by:

$$f_{i,k} = \frac{N_k d_k \left(c_i - x_{i,k} c_i^*\right) / \left(\beta_k + 1\right)}{\sum_{l=1}^{m} N_l d_l \left(c_i - x_{i,l} c_i^*\right) / \left(\beta_l + 1\right)}, \qquad \text{(E4)}$$

where N_k and d_k are the number and mean diameter of particles in mode k, m is the total number of aerosol modes, $\beta_k = 2\lambda/\alpha d_k$, α is the aerosol accommodation coefficient, and λ is the mean free path of air molecules (Pandis et al., 1993). This equation is solved iteratively at each time step and determines the OA composition of each mode. Overall, users may employ up to three hydrophilic modes (Aitken, accumulation, coarse) for the size distribution of all OA surrogate species. The ORACLE-lite version can also be applied using only accumulation mode to further reduce computational cost.

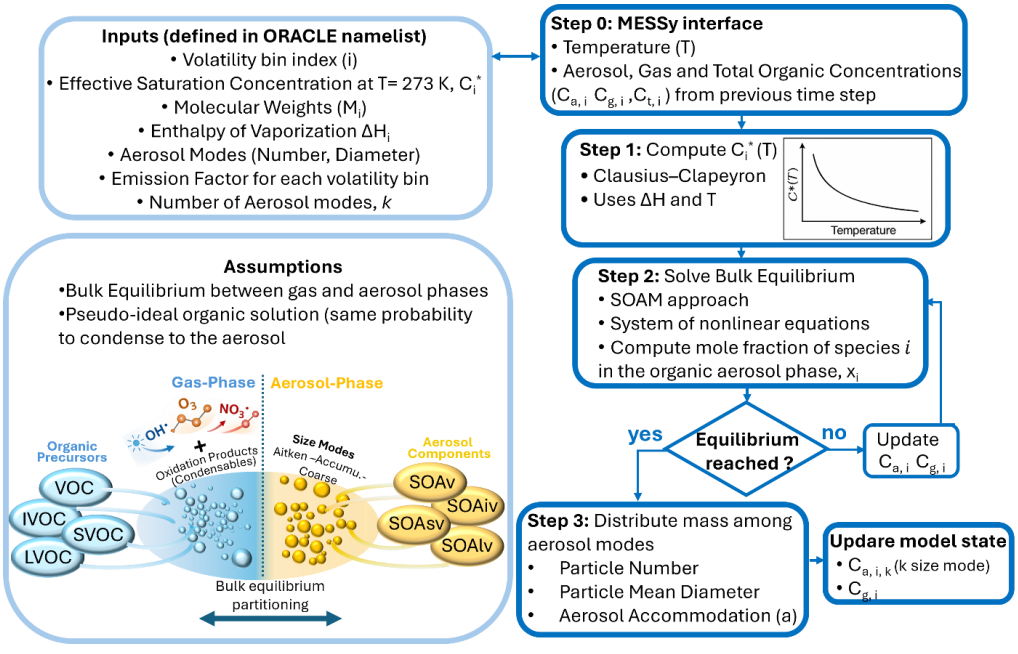

Figure 3: Schematic overview of the ORACLE-lite secondary organic aerosol (SOA) framework and its computational gas–particle partitioning workflow.

https://doi.org/10.5194/egusphere-2026-1709
Preprint. Discussion started: 8 April 2026

3. Evaluation of ORACLE-lite

3.1 Comparison of ORACLE-lite against ORACLE-base

3.1.1 Primary Organic Aerosol

Figure 4a depicts the global annual mean concentration of POA simulated by the ORACLE-lite model for 2010. The spatial distribution indicates that the highest concentrations are localized over well-known global hotspots of primary aerosol emissions. High concentrations (~10 μg m^{-3}) are simulated over Eastern China, reflecting substantial anthropogenic and industrial sources, extending into South Asia (e.g., India) and Southeast Asia. Two distinct, high-intensity plumes are also simulated over Equatorial and Southern Africa, associated with large-scale biomass burning in those regions. Other noticeable, though less intense, hotspots appear over parts of the Amazon Basin, also linked to biomass burning, with minor peaks over the Eastern United States and parts of Europe. Conversely, most of the global background atmosphere, including the oceans and remote continental areas, exhibits very low concentrations, generally below 2 μg m^{-3}, due to the relatively short atmospheric lifetime and limited long-range transport of POA.

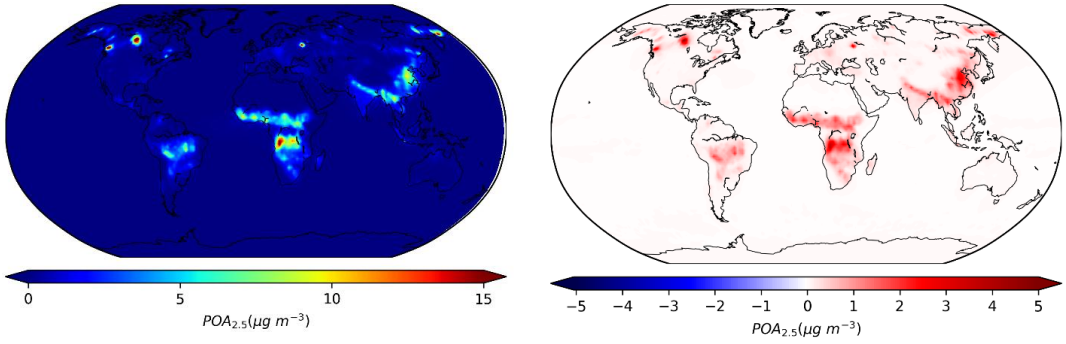

Figure 4: (a) Global annual mean concentration of POA for 2010 as simulated by ORACLE-lite. (b) Difference in POA concentration between ORACLE-lite and ORACLE-base simulations for the same period. Red colors indicate regions where ORACLE-lite predicts higher POA concentrations than ORACLE-base.

Figure 4b illustrates the absolute difference in POA concentration between ORACLE-lite and ORACLE-base. ORACLE-lite produces higher concentrations compared to the base model over areas with high POA emissions. Strong positive differences (up to 5 μg m^{-3}) are found over extensive biomass burning areas in Central and Southern Africa and across Eastern Asia. This is directly attributable to the different treatment of SVOCs in the two schemes. ORACLE-lite uses a single surrogate species for SVOC emissions with C* = 10^1 μg m^{-3}, whereas ORACLE-base uses two surrogate species with C* values of 10^0 and 10^2 μg m^{-3}. In regions with high OA concentrations, such as biomass burning areas in Africa or highly polluted regions of Eastern Asia,

https://doi.org/10.5194/egusphere-2026-1709
Preprint. Discussion started: 8 April 2026

the lower-volatility SVOC surrogate in ORACLE-lite preferentially partitions into the aerosol phase, producing more POA. In contrast, a significant portion of the SVOCs in ORACLE-base ($C^* = 10^2$ μg m^{-3}) remains in the gas phase. Broad positive differences are also observed across Northern Hemisphere mid-latitudes. These patterns highlight how the simplified VBS scheme in ORACLE-lite, particularly its choice of volatility bin, enhances POA concentrations over major source regions. In regions with lower OA concentrations (e.g., Europe and North America), ORACLE-lite and ORACLE-base predictions are similar, with differences below 1 μg m^{-3}.

3.1.2 Secondary Organic Aerosol

Figure 5a shows the global annual mean concentration of SOA simulated by ORACLE-lite for 2010. The spatial distribution of SOA differs from POA, reflecting its formation from the oxidation of gas-phase organic compounds (SVOCs, IVOCs, VOCs) downwind of emission sources. The highest concentrations, generally exceeding 10 μg m^{-3}, occur over Eastern China and India, regions characterized by substantial anthropogenic emissions and high photochemical activity. Significant plumes are also observed over tropical forest regions in the Amazon Basin and Equatorial Africa, driven by biogenic VOCs and biomass burning IVOCs and SVOCs, followed by subsequent SOA formation. Compared to POA, SOA plumes are more diffuse and spatially extended, reflecting its secondary nature and longer atmospheric lifetime, which allows for greater transport from precursor emission regions. Southern oceans, however, maintain very low background concentrations.

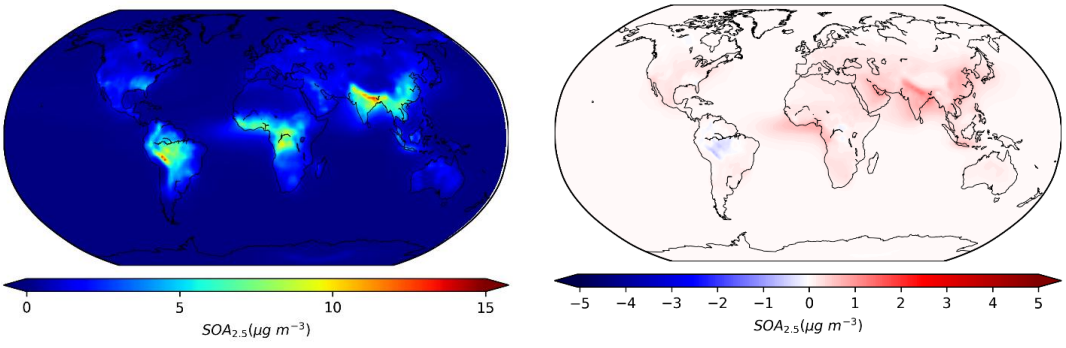

Figure 5: (a) Global annual mean concentration of SOA for 2010 as simulated by ORACLE-lite. (b) Difference in SOA concentration between ORACLE-lite and ORACLE-base simulations. Red indicates higher concentrations in ORACLE-lite; blue indicates lower concentrations.

Figure 5b presents the absolute difference in SOA concentration between ORACLE-lite and ORACLE-base. Differences show a clear spatial pattern driven by the models' treatment of volatility bins for SOA precursors. ORACLE-lite predicts higher SOA concentrations over densely populated and industrialized regions, notably Eastern China, the Middle East, and Europe. This increase is primarily associated with SOA-v (Figure S1). The simplified VBS scheme in ORACLE-lite, with fewer volatility bins, allocates more aerosol yield to the lower-volatility bin

https://doi.org/10.5194/egusphere-2026-1709
Preprint. Discussion started: 8 April 2026

($C^* = 10^0$ μg m^{-3}), causing a larger fraction of condensable organic mass from VOC oxidation to partition into the aerosol phase, enhancing SOA formation in regions with high precursor concentrations. Conversely, ORACLE-lite predicts lower SOA concentrations over major biomass burning regions, particularly the Amazon Basin and parts of Southern Africa. This is a direct consequence of the enhanced POA formation in these regions. More SVOCs partition into POA, leaving less material available for gas-phase oxidation and SOA production (Figure S1). Therefore, ORACLE-base, which retains more SVOCs in the gas phase, produces higher SOA concentrations over biomass burning areas.

3.1.3 Computational performance and efficiency

To quantify the computational benefits of the simplified volatility basis set, we evaluated the performance of ORACLE-lite relative to the standard ORACLE-base configuration. Table 2 summarizes the total number of model time steps completed during fixed wallclock simulations, as well as the average computational cost per time step. ORACLE-lite requires 1.44 ± 0.02 s per time step, compared to 1.67 ± 0.01 s for ORACLE-base, corresponding to a computational speed-up of approximately 14%. This improvement reflects the reduced number of tracers and the simplified representation of volatility evolution in ORACLE-lite, which decreases the computational burden associated with gas–particle partitioning and chemical aging calculations.

As a result, ORACLE-lite performs a larger number of time steps within the same wallclock time (~57 000 vs. ~49 000 steps in 24 h of CPU time), indicating a substantial gain in numerical efficiency. This speed-up is particularly important for multi-decadal chemistry-climate simulations, where computational cost is a primary limiting factor. Since the total computational cost of EMAC is distributed among several processes, including gas-phase chemistry, aerosol microphysics, and transport, the improvement introduced by ORACLE-lite translates into a meaningful enhancement of overall model performance.

These results demonstrate that ORACLE-lite provides a significant computational advantage while maintaining the ability to simulate the key features of organic aerosol formation and evolution, supporting its application in long-term climate simulations.

Table 2. Computational performance metrics for ORACLE-lite and ORACLE-base. Values represent the mean ± standard deviation, calculated from a total of 12 simulations (6 for each configuration). The number of time steps corresponds to the total steps completed within 24 h of CPU time using 16 nodes.

Simulation	No. of time steps	Time per step (s)	Relative speed-up (%)
ORACLE-lite	57 053 ± 718	1.439 ± 0.018 s	13.9 ± 1.1 %
ORACLE-BASE	49 066 ± 310	1.673 ± 0.011 s	-

https://doi.org/10.5194/egusphere-2026-1709
Preprint. Discussion started: 8 April 2026

3.2 Model performance evaluation against AMS observations

3.2.1 Total Organic Aerosol

Figure 6 presents the spatial distribution of the relative deviation (%) between EMAC-simulated and observed PM_1 OA concentrations based on AMS and ACSM datasets. Overall, the model reproduces the large-scale spatial variability of OA across regions, with most locations showing agreement within a factor of two. The spatial distribution of biases exhibits clear regional patterns, with relatively good agreement over North America and parts of Eastern Asia, while more pronounced deviations are found over Europe and tropical regions. The model generally tends to underestimate OA concentrations, especially over Europe, although localized overestimations are observed, particularly over parts of Africa and Latin America. These spatial patterns reflect regional differences in emission sources, atmospheric processing, and remaining limitations in the representation of OA formation pathways.

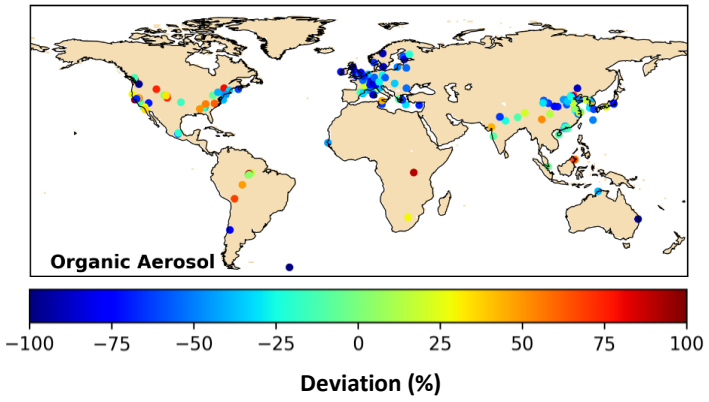

Figure 6: Deviations (in %) between EMAC simulated and observed OA, based on AMS and ACSM datasets over the period 2000 – 2020. Negative values (blue colors) indicate underprediction of OA concentrations by the model.

Consistent with the spatial patterns shown in Figure 6, the model performance for total OA concentrations varies substantially across continents. Over North America, the simulated mean OA agrees well with AMS observations (NMB = –4%). However, the comparison shows considerable scatter (NME = 64%), as the model tends to overpredict OA at rural locations (NMB = 37%) and underpredict it over and downwind of urban sites (NMB = –28%). The model broadly captures the observed seasonality of OA over North America, with higher concentrations in summer and autumn and lower levels in spring and winter. OA peaks in summer due to enhanced biogenic VOC emissions and photochemical activity (Goldstein and Galbally, 2007; Tsimpidi et al., 2016). Nevertheless, EMAC overestimates some of the low summertime OA concentrations measured by AMS at several rural sites (Figure 7a).

Over Europe, the model generally underestimates OA during all seasons except summer (Figure 7b). Model performance is poorest in winter, when biomass-burning emissions, particularly from residential wood combustion, and their dark oxidation have been identified as major contributors to model bias (Tsimpidi et al., 2016; Kodros et al., 2020). This bias also affects the simulated OA

https://doi.org/10.5194/egusphere-2026-1709
Preprint. Discussion started: 8 April 2026

seasonality. The model predicts higher OA concentrations in summer across all environments, whereas AMS observations show that this pattern applies only to rural sites. According to AMS data, OA concentrations over and downwind of urban areas peak in winter.

Over East Asia, the model performs best, with relatively low bias (NMB = –29%) and scatter (NME = 49%). In contrast to Europe, wintertime OA is well captured, even at urban locations (Table 3). Model performance is particularly strong over rural and urban-downwind areas, with 75% of data points within a factor of two from observations. However, as is typical for global models (Tsigaridis et al., 2014), the model fails to reproduce some of the high OA concentrations observed in major urban centers due to limited spatial resolution (Figure 7c).

Table 3: Statistical evaluation of EMAC-simulated PM_1 OA concentrations against AMS and ACSM observations over 2000–2020. Results are shown for Europe, North America, Eastern Asia, and tropical and subtropical regions. The first three regions are further divided into rural, downwind, and urban sites, while tropical and subtropical regions are subdivided into Latin America and the Caribbean, Africa, South Asia and Developing Pacific, and Asia-Pacific developed regions.

Continent	Region	Number of data sets	Mean observed (μg m^{-3})	Mean predicted (μg m^{-3})	MAGE (μg m^{-3})	MB (μg m^{-3})	NME (%)	NMB (%)	RMSE (μg m^{-3})
Europe	all	442	4.6	2.2	2.7	-2.4	59.5	-52.6	4.0
	rural	247	3.6	2.00	2.1	-1.6	58.2	-45.9	3.1
	downwind	156	5.9	2.5	3.7	-3.4	61.6	-58.6	5.1
	urban	39	5.3	2.5	3.0	-2.8	56.4	-54.1	3.7
North America	all	86	4.8	4.6	3.1	-0.2	64.1	-4.2	4.3
	rural	46	3.3	4.5	3.0	1.2	89.8	37.3	4.5
	downwind	7	5.6	4.6	2.3	-1.0	41.0	-17.4	2.9
	urban	33	6.7	4.6	3.4	-2.0	50.5	-30.5	4.2
Eastern Asia	all	159	19.3	13.6	9.4	-5.7	48.7	-29.3	13.2
	rural	44	12.8	10.8	6.7	-2.0	52.6	-15.8	11.6
	downwind	16	11.4	9.8	6.0	-1.6	52.7	-14.0	8.9
	urban	99	23.5	15.6	11.2	-7.9	47.5	-33.8	14.4
Tropical and Subtropical	all	75	14.5	8.9	9.3	-5.6	63.3	-39.0	14.7
	S America	21	8.4	5.5	5.5	-2.9	65.0	-34.4	8.12
	Africa	14	3.4	5.5	2.4	2.1	70.3	61.0	3.3
	SE Asia	23	33.3	18.6	19.2	-14.7	57.9	-44.0	28.99
	Pacific	17	5.8	2.5	3.4	-3.3	58.6	-56.1	4.64

The comparison between simulated and observed OA concentrations across tropical and subtropical regions (Figure 7d) shows that the model captures the overall magnitude and variability of OA, with most data points falling within a factor of two of the observations. On average, the model underestimates OA concentrations, indicating a moderate negative bias (MB = −5.6 μg m^{-3}) accompanied by substantial scatter (NME=63%). However, systematic regional differences are evident. Over South Asia and the Developing Pacific, the model captures the general variability across seasons (Figure S1) but systematically underestimates higher observed concentrations,

https://doi.org/10.5194/egusphere-2026-1709
Preprint. Discussion started: 8 April 2026

suggesting limitations in representing strong emission sources and/or secondary formation pathways. A consistent underestimation is also observed over the Asia-Pacific Developed region, similar to that found in other developed regions.

In contrast, over Africa, the model shows a pronounced positive bias (NMB = 61.0%). This overestimation is most evident during the dry season and likely reflects enhanced partitioning of semi-volatile organic compounds into the particle phase in biomass-burning regions, consistent with the elevated POA concentrations in these areas. Over Latin America and the Caribbean, the model exhibits relatively large scatter (NME ≈ 65%), indicating substantial variability across sites and seasons. While the model captures the overall range of observed concentrations, it tends to overestimate OA during the Amazonian wet season and underestimate it during the dry season, highlighting challenges in representing both biogenic secondary organic aerosol formation and seasonal emission variability.

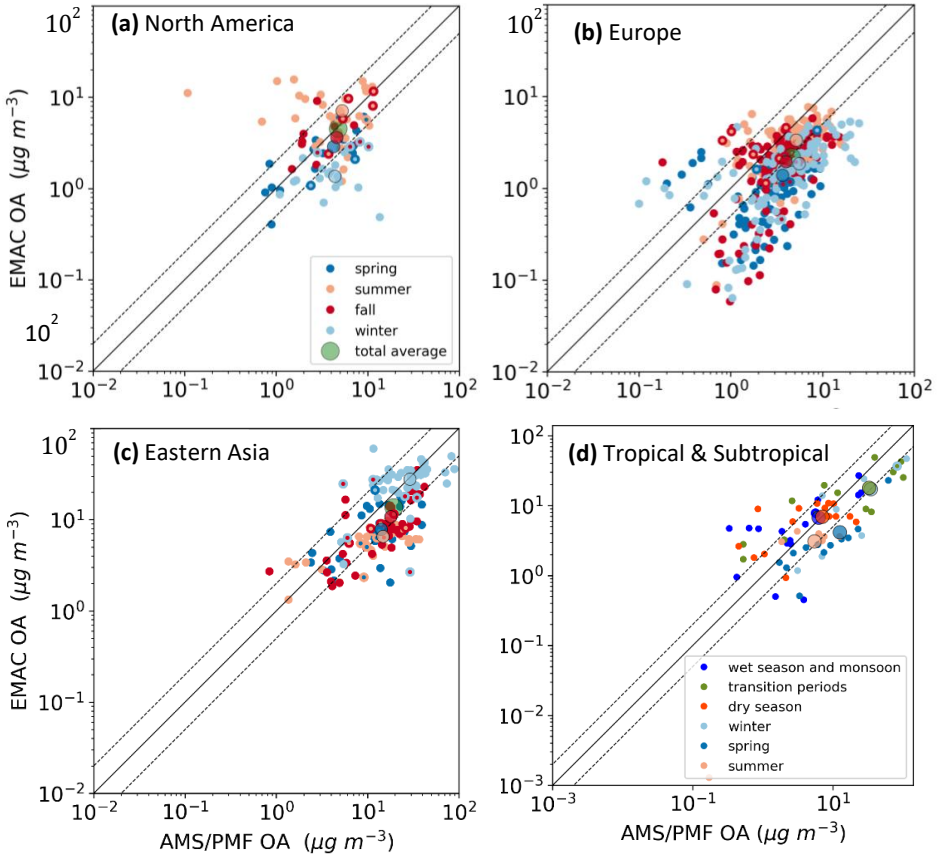

Figure 7: Scatter plots comparing EMAC simulated PM_1 OA concentrations (μg m^{-3}) with AMS and ACSM observations over (a) North America, (b) Europe, (c) Eastern Asia, and (d) tropical and subtropical regions. Each point represents the mean OA concentration of an individual dataset. Points are colored by season of the field campaign. Solid and dashed lines indicate the 1:1, 2:1, and 1:2 relationships.

https://doi.org/10.5194/egusphere-2026-1709
Preprint. Discussion started: 8 April 2026

3.2.2 Primary Organic Aerosol

The simulated POA concentrations are compared with the sum of AMS HOA and BBOA. POA concentrations are generally underestimated by the model over North America and Europe (NMB ≈ -45%) and strongly overestimated over Eastern Asia (NMB = 98%). In North American rural regions, simulated POA concentrations are highest during spring and winter and lowest during autumn, consistent with the observed seasonality. However, during summer the model underestimates most observed POA values (Figure 8). Over urban locations, POA is even more severely underestimated (NMB = –68%), largely due to the coarse spatial resolution of the model and the evaporation of organic compounds upon emission.

In Europe, POA is also underestimated over urban regions (NMB = -52%), although the bias is smaller than in North America. Over rural areas, model performance is highly scattered across all seasons, with several cases of substantial over and underprediction (NME = 62%).

Over Eastern Asia, a pronounced overestimation is evident during winter, particularly over megacity clusters such as those around Hong Kong and Shanghai (NMB = 106%; Table 4). This discrepancy may be partly attributable to biases in the emission inventory (e.g., the lack of representation of emission reductions associated with recent Chinese clean air action plans) and partly to an excessive partitioning of freshly emitted SVOCs into the particle phase under cold winter conditions. Tsimpidi et al. (2016) also reported POA overestimations in Eastern Asia, attributed in part to high simulated biomass burning POA transported from surrounding boreal forests. Since POA in ORACLE does not participate in aqueous-phase or other heterogeneous reactions, it does not convert to SOA through these pathways, which may further contribute to the positive model bias during winter.

Table 4: Statistical evaluation of EMAC PM_1 POA concentrations against AMS and ACSM datasets over Europe, North America, and Eastern Asia during 2000–2020.

Continent	Region	Number of data sets	Mean observed (μg m⁻³)	Mean predicted (μg m⁻³)	MAGE (μg m⁻³)	MB (μg m⁻³)	NME (%)	NMB (%)	RMSE (μg m⁻³)
Europe	all	106	1.18	0.67	0.81	-0.51	68.45	-43.27	1.60
	rural	62	0.90	0.49	0.56	-0.40	62.50	-44.78	1.13
	downwind	23	1.70	1.12	1.38	-0.58	81.24	-34.19	2.60
	urban	21	1.45	0.69	0.91	-0.75	62.87	-52.20	1.32
North America	all	50	1.17	0.63	0.95	-0.54	80.93	-46.20	1.49
	rural	21	0.62	0.64	0.65	0.02	106.18	3.64	1.59
	downwind	3	0.41	1.27	1.16	0.86	284.25	212.29	1.76
	urban	26	1.70	0.55	1.16	-1.16	67.93	-67.93	1.38
Eastern Asia	all	129	4.88	9.91	6.89	5.03	141.12	103.18	11.40
	rural	35	5.10	9.28	6.11	4.18	119.82	82.03	11.38
	downwind	13	3.68	5.91	3.80	2.23	103.00	60.49	5.82
	urban	81	4.98	10.83	7.72	5.85	155.08	117.62	12.07

https://doi.org/10.5194/egusphere-2026-1709
Preprint. Discussion started: 8 April 2026

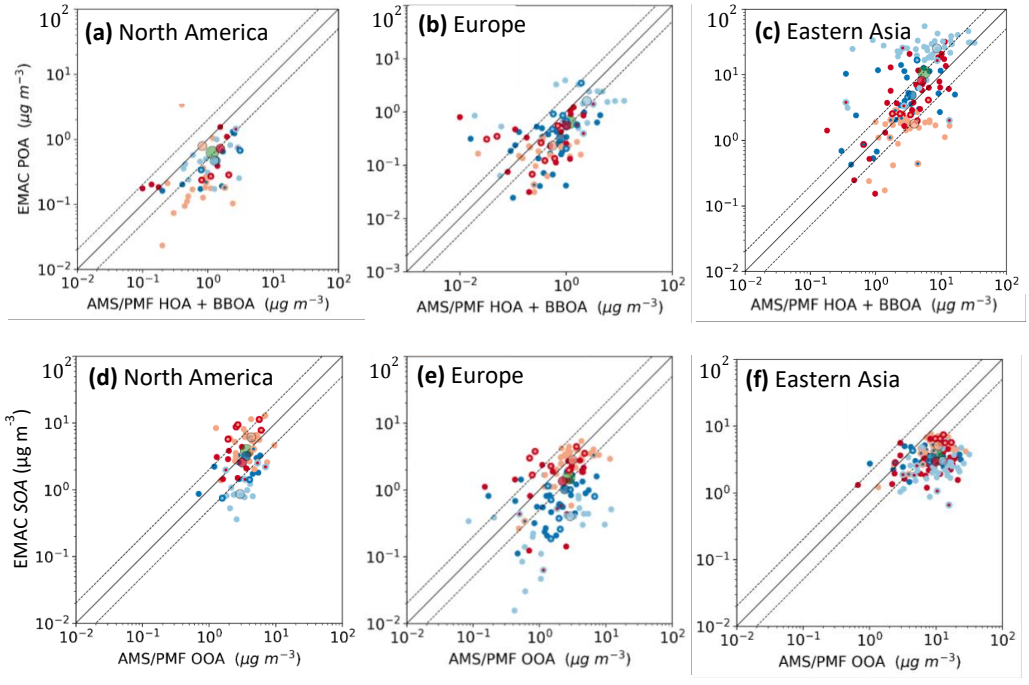

Figure 8: Scatter plots comparing model results for PM_1 POA (a-c) and secondary organic aerosol (d-f) concentrations (in μg m^{-3}) with AMS and ACSM observations of HOA+BOA and OOA, respectively, over North America (a, d), Europe (b, e), and Eastern Asia (c, f). Each point represents the data set mean and is colored based on the season of the field campaign. Also shown are the 1:1, 2:1, and 1:2 lines.

3.2.3 Secondary Organic Aerosol

The simulated OOA concentrations over North America agree very well with the OOA derived from the PMF analysis of AMS observations (NMB = 4.5%). The model performs well across both urban and rural areas and during all seasons, except winter, when it tends to underpredict AMS-OOA (Table 5; Figure 8d). L-OOA concentrations are reproduced particularly well (Figure 9a; Table S1), whereas M-OOA concentrations are slightly underestimated during spring and autumn and substantially underpredicted during winter (Figure 9d, Table S2).

Similarly, over Europe, the model performance for all OOA types is best during summer and worst during winter, when it underestimates the AMS-derived concentrations, especially for M-OOA (Figure 9e). During summer, high temperatures enhance biogenic VOC emissions and the abundant solar radiation promotes photochemical processing, which efficiently converts gas-phase

https://doi.org/10.5194/egusphere-2026-1709
Preprint. Discussion started: 8 April 2026

Table 5: Statistical evaluation of EMAC PM_1 SOA concentrations against AMS and ACSM datasets over Europe, North America, and Eastern Asia during 2000–2020.

Continent	Region	Number of data sets	Mean observed (μg m^{-3})	Mean predicted (μg m^{-3})	MAGE (μg m^{-3})	MB (μg m^{-3})	NME (%)	NMB (%)	RMSE (μg m^{-3})
Europe	all	129	2.77	1.51	1.69	-1.26	61.01	-45.60	2.44
	rural	84	2.53	1.52	1.53	-1.01	60.54	-39.93	2.34
	downwind	24	3.43	1.19	2.41	-2.24	70.17	-65.19	3.15
	urban	21	2.98	1.81	1.50	-1.16	50.55	-39.09	1.83
North America	all	67	3.66	3.83	2.34	0.17	63.89	4.52	3.00
	rural	35	3.16	3.51	2.11	0.35	66.92	11.08	2.79
	downwind	6	5.27	4.23	2.33	-1.05	44.25	-19.87	3.05
	urban	26	3.97	4.17	2.65	0.20	66.66	4.97	3.24
Eastern Asia	all	147	10.65	3.54	7.23	-7.11	67.86	-66.74	9.24
	rural	36	8.18	3.38	5.29	-4.80	64.62	-58.69	7.15
	downwind	16	7.84	4.03	3.82	-3.82	48.68	-48.68	5.23
	urban	95	12.06	3.52	8.53	-8.53	70.79	-70.79	10.41

organic compounds into particulate OOA (Seco et al., 2011; Xu et al., 2017; Tsimpidi et al., 2016). Good model performance during summer indicates that the model captures these processes reasonably well. In winter, however, photochemical processing plays a much smaller role in OOA formation (Xu et al., 2017). As temperatures and photochemical activity decrease, the model performance deteriorates, indicating that additional formation pathways become increasingly important.

Key missing SOA formation pathways include heterogeneous reactions such as oligomerization and aqueous-phase processing (Hallquist et al., 2009; Tsimpidi et al., 2016). Under high RH conditions, aqueous-phase reactions can rapidly generate highly oxidized OOA (i.e., M-OOA with high O:C), while their impact on fresher, less oxidized OOA (i.e., L-OOA) is relatively minor. For L-OOA, gas-phase photochemical aging under low RH is more important (Xu et al., 2017). Although these processes occur year-round, winter meteorological conditions strongly favor M-OOA formation via aqueous-phase chemistry over L-OOA formation via gas-phase oxidation (Xu et al., 2017; Mortier et al., 2020; Pozzer et al., 2022). As a result, the missing aqueous-phase pathway becomes increasingly important from spring and autumn to winter. Additionally, recent studies have shown substantial SOA production in winter due to the rapid nighttime oxidation of biomass-burning OA by the NO_3 radical (Kodros et al., 2020; Paglione et al., 2020; Liu, 2024). Because emissions from residential wood burning are not included in the model and ORACLE simulates only the predominant OH-driven photochemical processing of BBOA, the absence of dark oxidation pathways likely contributes to the significant wintertime underprediction of OOA.

Over Eastern Asia, OOA is underestimated even during summer (Figure 9f), mainly due to the underprediction of M-OOA, while L-OOA is reproduced reasonably well in all seasons (Figure 9).

https://doi.org/10.5194/egusphere-2026-1709
Preprint. Discussion started: 8 April 2026

Eastern Asia experiences high RH even in summer, reinforcing the hypothesis that aqueous-phase processes represent an important missing mechanism for SOA formation. Recent studies have shown that the uptake of water-soluble gas-phase oxidation products, even small carbonyls such as formaldehyde and acetic acid, followed by aqueous-phase oxidation and oligomerization, can significantly increase SOA mass during pollution events (Gkatzelis et al., 2021). Overall, EMAC performs best over Eastern Asian rural areas during summer and spring and worst near urban regions during autumn and winter. Particularly in winter, the model reproduces total OA reasonably well but strongly overpredicts POA (Figure 8c) while underpredicting SOA (especially M-OOA). This inconsistency likely reflects both an overestimation of POA formation from emitted SVOCs and the absence of a mechanism that efficiently converts POA to SOA within the aerosol phase under winter conditions.

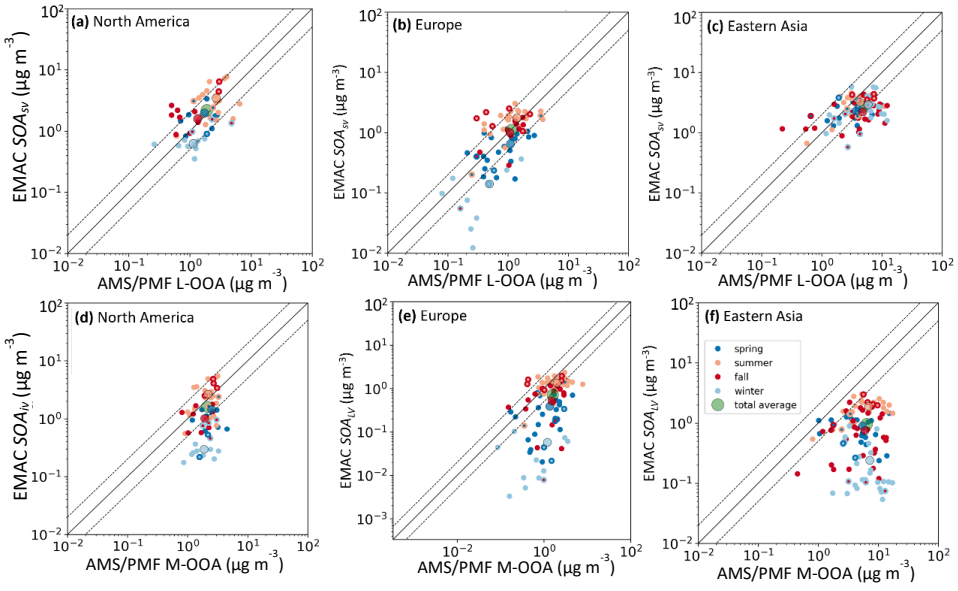

Figure 9: Scatter plots comparing model results for PM_1 SOA_{sv} (a-c) and SOA_{iv} (d-f) concentrations (in µg m^{-3}) with AMS and ACSM observations of L-OOA and M-OOA, respectively, over North America (a, d), Europe (b, e), and Eastern Asia (c, f). Each point represents the data set mean and is colored based on the season of the field campaign. Also shown are the 1:1, 2:1, and 1:2 lines.

4 Conclusions

In this study, we introduced ORACLE-lite (v3.0), a reduced-complexity organic aerosol (OA) module implemented in the EMAC chemistry–climate model, designed specifically for multi-decadal simulations. ORACLE-lite preserves the key processes governing OA formation and multi-generational aging while employing a minimal set of surrogate species to represent the volatility distribution of organic compounds.

https://doi.org/10.5194/egusphere-2026-1709
Preprint. Discussion started: 8 April 2026

The comparison with the standard ORACLE-base configuration demonstrates that the simplified volatility basis set in ORACLE-lite leads to physically interpretable changes in OA partitioning. The use of a reduced number of volatility bins enhances the gas–particle partitioning of freshly emitted semi-volatile material, resulting in higher primary organic aerosol (POA) concentrations over major emission regions, particularly biomass-burning areas and highly polluted anthropogenically influenced regions such as Eastern Asia. At the same time, the redistribution of semi-volatile material between phases modifies secondary organic aerosol (SOA) formation, leading to decreased SOA over biomass-burning regions. In contrast, SOA formation is enhanced over regions dominated by anthropogenic VOC emissions. Despite these differences, ORACLE-lite successfully reproduces the global spatial patterns and relative contributions of POA and SOA.

Evaluation against long-term AMS and ACSM observations indicates that ORACLE-lite captures the magnitude, spatial distribution, and seasonal variability of total OA across major regions. Model performance is particularly strong over North America and Eastern Asia, where simulated OA concentrations agree well with observations and most data fall within a factor of two. Across tropical and subtropical regions, the model also reproduces OA variability within a factor of two for the majority of observations, although it exhibits a moderate overall underestimation and substantial regional variability. The model also reproduces key features of OA composition, including the relative contributions of primary and secondary components. Remaining discrepancies, such as the underestimation of wintertime SOA and biases in Europe, are consistent with known limitations of global models, including uncertainties in emissions and the absence of certain formation pathways such as aqueous-phase processing and nighttime chemistry. Region-specific biases, such as the overestimation over biomass-burning regions in Africa and the underestimation in South and Southeast Asia, further highlight the sensitivity of OA to emission strength, volatility distribution, and missing chemical pathways.

A key advantage of ORACLE-lite is its improved computational efficiency. The simplified representation reduces the computational cost per model time step by approximately 14%, allowing a substantially larger number of time steps to be simulated within a fixed wallclock time. This gain is achieved without sacrificing the physically based representation of OA formation and evolution, making ORACLE-lite particularly suitable for long-term chemistry–climate applications where computational cost is a critical constraint.

Overall, ORACLE-lite provides an effective balance between process representation and computational efficiency. By retaining the essential features of volatility-based OA formation while significantly reducing model complexity, it enables robust and physically grounded simulations of organic aerosol over decadal timescales. This makes ORACLE-lite a valuable tool for investigating the role of organic aerosol in air quality and climate, as well as for exploring future emission and climate scenarios in global chemistry–climate models.

Code and data availability. The usage of MESSy (Modular Earth Submodel System) and access to the source code is licensed to all affiliates of institutions which are members of the MESSy Consortium. Institutions can become members of the MESSy Consortium by signing the MESSy Memorandum of Understanding. More information can be found on the MESSy Consortium Website http://www.messy-interface.org. The code developed in this study is archived with a restricted access https://zenodo.org/records/19204803 (MESSy Consortium, 2026) and has already

https://doi.org/10.5194/egusphere-2026-1709
Preprint. Discussion started: 8 April 2026

been incorporated into the official development branch of the EMAC modelling system and will therefore be part of all future released versions.

Authors contributions: APT and VAK contributed equally to all aspects of this work, including study design, model development, simulations, analysis, and manuscript preparation.

Competing interests: The authors declare that they have no conflict of interest.

Acknowledgements: The work described in this paper was supported by the European Research Council by the Union's Horizon 2020 research and innovation programme (FORCeS, grant No. 821205) and the Initiative and Networking Fund of the Helmholtz Association through the project *Advanced Earth System Modelling Capacity (ESM)*. We acknowledge the EBAS database (https://ebas.nilu.no), operated by NILU – Norwegian Institute for Air Research, for providing part of the observational data used in this study. We also acknowledge the numerous data providers, measurement networks, and research groups worldwide that contributed AMS and ACSM observations used for model evaluation. The authors gratefully acknowledge the Earth System Modelling project (ESM) for providing computing time on the ESM partition of the supercomputer JUWELS at the Jülich Supercomputing Centre (JSC), Forschungszentrum Jülich (Alvarez, 2021).

References

Alvarez, D.: JUWELS Cluster and Booster: Exascale Pathfinder with Modular Supercomputing Architecture at Juelich Supercomputing Centre, Journal of large-scale research facilities JLSRF, 7, 10.17815/jlsrf-7-183, 2021.

Bergstrom, R., van der Gon, H. A. C. D., Prevot, A. S. H., Yttri, K. E., and Simpson, D.: Modelling of organic aerosols over Europe (2002-2007) using a volatility basis set (VBS) framework: application of different assumptions regarding the formation of secondary organic aerosol, Atmos. Chem. Phys., 12, 8499-8527, 2012.

Bianchi, F., Kurtén, T., Riva, M., Mohr, C., Rissanen, M. P., Roldin, P., Berndt, T., Crounse, J. D., Wennberg, P. O., Mentel, T. F., Wildt, J., Junninen, H., Jokinen, T., Kulmala, M., Worsnop, D. R., Thornton, J. A., Donahue, N., Kjaergaard, H. G., and Ehn, M.: Highly Oxygenated Organic Molecules (HOM) from Gas-Phase Autoxidation Involving Peroxy Radicals: A Key Contributor to Atmospheric Aerosol, Chemical Reviews, 119, 3472-3509, 10.1021/acs.chemrev.8b00395, 2019.

Browne, E. C., Min, K. E., Wooldridge, P. J., Apel, E., Blake, D. R., Brune, W. H., Cantrell, C. A., Cubison, M. J., Diskin, G. S., Jimenez, J. L., Weinheimer, A. J., Wennberg, P. O., Wisthaler, A., and Cohen, R. C.: Observations of total RONO2 over the boreal forest: NOx sinks and HNO3 sources, Atmos. Chem. and Phys., 13, 4543-4562, 2013.

Donahue, N. M., Epstein, S. A., Pandis, S. N., and Robinson, A. L.: A two-dimensional volatility basis set: 1. organic-aerosol mixing thermodynamics, Atmos. Chem. and Phys., 11, 3303-3318, 2011.

Donahue, N. M., Kroll, J. H., Pandis, S. N., and Robinson, A. L.: A two-dimensional volatility basis set - Part 2: Diagnostics of organic-aerosol evolution, Atmos. Chem. Phys., 12, 615-634, 2012a.

Donahue, N. M., Robinson, A. L., Stanier, C. O., and Pandis, S. N.: Coupled partitioning, dilution, and chemical aging of semivolatile organics, Environ. Sci. Technol., 40, 2635-2643, 2006.

Donahue, N. M., Chuang, W., Epstein, S. A., Kroll, J. H., Worsnop, D. R., Robinson, A. L., Adams, P. J., and Pandis, S. N.: Why do organic aerosols exist? Understanding aerosol lifetimes using the two-dimensional volatility basis set, Environ. Chem., 10, 151-157, 2013.

Donahue, N. M., Henry, K. M., Mentel, T. F., Kiendler-Scharr, A., Spindler, C., Bohn, B., Brauers, T., Dorn, H. P., Fuchs, H., Tillmann, R., Wahner, A., Saathoff, H., Naumann, K.-H., Moehler, O., Leisner, T., Mueller, L., Reinnig, M.-C., Hoffmann, T., Salo, K., Hallquist, M., Frosch, M., Bilde, M., Tritscher, T., Barmet, P., Praplan, A. P., DeCarlo, P. F., Dommen, J., Prevot, A. S. H., and Baltensperger, U.:

https://doi.org/10.5194/egusphere-2026-1709
Preprint. Discussion started: 8 April 2026

Aging of biogenic secondary organic aerosol via gas-phase OH radical reactions, Proceedings of the National Academy of Sciences of the United States of America, 109, 13503-13508, 10.1073/pnas.1115186109, 2012b.

Ehn, M., Thornton, J. A., Kleist, E., Sipila, M., Junninen, H., Pullinen, I., Springer, M., Rubach, F., Tillmann, R., Lee, B., Lopez-Hilfiker, F., Andres, S., Acir, I.-H., Rissanen, M., Jokinen, T., Schobesberger, S., Kangasluoma, J., Kontkanen, J., Nieminen, T., Kurten, T., Nielsen, L. B., Jorgensen, S., Kjaergaard, H. G., Canagaratna, M., Maso, M. D., Berndt, T., Petaja, T., Wahner, A., Kerminen, V.-M., Kulmala, M., Worsnop, D. R., Wildt, J., and Mentel, T. F.: A large source of low-volatility secondary organic aerosol, Nature, 506, doi: 10.1038/nature13032, 2014.

Gkatzelis, G. I., Papanastasiou, D. K., Karydis, V. A., Hohaus, T., Liu, Y., Schmitt, S. H., Schlag, P., Fuchs, H., Novelli, A., Chen, Q., Cheng, X., Broch, S., Dong, H., Holland, F., Li, X., Liu, Y. H., Ma, X. F., Reimer, D., Rohrer, F., Shao, M., Tan, Z., Taraborrelli, D., Tillmann, R., Wang, H. C., Wang, Y., Wu, Y. S., Wu, Z. J., Zeng, L. M., Zheng, J., Hu, M., Lu, K. D., Hofzumahaus, A., Zhang, Y. H., Wahner, A., and Kiendler-Scharr, A.: Uptake of Water-soluble Gas-phase Oxidation Products Drives Organic Particulate Pollution in Beijing, Geophysical Research Letters, 48, 10.1029/2020gl091351, 2021.

Goldstein, A. H. and Galbally, I. E.: Known and unexplored organic constituents in the earth's atmosphere, Environmental Science & Technology, 41, 1514-1521, 10.1021/es072476p, 2007.

Hallquist, M., Wenger, J. C., Baltensperger, U., Rudich, Y., Simpson, D., Claeys, M., Dommen, J., Donahue, N. M., George, C., Goldstein, A. H., Hamilton, J. F., Herrmann, H., Hoffmann, T., Iinuma, Y., Jang, M., Jenkin, M. E., Jimenez, J. L., Kiendler-Scharr, A., Maenhaut, W., McFiggans, G., Mentel, T. F., Monod, A., Prevot, A. S. H., Seinfeld, J. H., Surratt, J. D., Szmigielski, R., and Wildt, J.: The formation, properties and impact of secondary organic aerosol: current and emerging issues, Atmospheric Chemistry and Physics, 9, 5155-5236, 10.5194/acp-9-5155-2009, 2009.

Hodzic, A. and Jimenez, J. L.: Modeling anthropogenically controlled secondary organic aerosols in a megacity: a simplified framework for global and climate models, Geosci. Model Dev., 4, 901-917, 10.5194/gmd-4-901-2011, 2011.

Hodzic, A., Kasibhatla, P. S., Jo, D. S., Cappa, C. D., Jimenez, J. L., Madronich, S., and Park, R. J.: Rethinking the global secondary organic aerosol (SOA) budget: stronger production, faster removal, shorter lifetime, Atmos. Chem. Phys., 16, 7917-7941, 10.5194/acp-16-7917-2016, 2016.

Hodzic, A., Campuzano-Jost, P., Bian, H. S., Chin, M., Colarco, P. R., Day, D. A., Froyd, K. D., Heinold, B., Jo, D. S., Katich, J. M., Kodros, J. K., Nault, B. A., Pierce, J. R., Ray, E., Schacht, J., Schill, G. P., Schroder, J. C., Schwarz, J. P., Sueper, D. T., Tegen, I., Tilmes, S., Tsigaridis, K., Yu, P. F., and Jimenez, J. L.: Characterization of organic aerosol across the global remote troposphere: a comparison of ATom measurements and global chemistry models, Atmospheric Chemistry and Physics, 20, 4607-4635, 10.5194/acp-20-4607-2020, 2020.

Jimenez, J. L., Canagaratna, M. R., Donahue, N. M., Prevot, A. S. H., Zhang, Q., Kroll, J. H., DeCarlo, P. F., Allan, J. D., Coe, H., Ng, N. L., Aiken, A. C., Docherty, K. S., Ulbrich, I. M., Grieshop, A. P., Robinson, A. L., Duplissy, J., Smith, J. D., Wilson, K. R., Lanz, V. A., Hueglin, C., Sun, Y. L., Tian, J., Laaksonen, A., Raatikainen, T., Rautiainen, J., Vaattovaara, P., Ehn, M., Kulmala, M., Tomlinson, J. M., Collins, D. R., Cubison, M. J., Dunlea, E. J., Huffman, J. A., Onasch, T. B., Alfarra, M. R., Williams, P. I., Bower, K., Kondo, Y., Schneider, J., Drewnick, F., Borrmann, S., Weimer, S., Demerjian, K., Salcedo, D., Cottrell, L., Griffin, R., Takami, A., Miyoshi, T., Hatakeyama, S., Shimono, A., Sun, J. Y., Zhang, Y. M., Dzepina, K., Kimmel, J. R., Sueper, D., Jayne, J. T., Herndon, S. C., Trimborn, A. M., Williams, L. R., Wood, E. C., Middlebrook, A. M., Kolb, C. E., Baltensperger, U., and Worsnop, D. R.: Evolution of organic aerosols in the atmosphere, Science, 326, 1525-1529, 2009.

Jöckel, P., Kerkweg, A., Pozzer, A., Sander, R., Tost, H., Riede, H., Baumgaertner, A., Gromov, S., and Kern, B.: Development cycle 2 of the Modular Earth Submodel System (MESSy2), Geoscientific Model Development, 3, 717-752, 2010.

Jöckel, P., Tost, H., Pozzer, A., Bruehl, C., Buchholz, J., Ganzeveld, L., Hoor, P., Kerkweg, A., Lawrence, M. G., Sander, R., Steil, B., Stiller, G., Tanarhte, M., Taraborrelli, D., Van Aardenne, J., and Lelieveld,

https://doi.org/10.5194/egusphere-2026-1709
Preprint. Discussion started: 8 April 2026

J.: The atmospheric chemistry general circulation model ECHAM5/MESSy1: consistent simulation of ozone from the surface to the mesosphere, Atmos. Chem. Phys., 6, 5067-5104, 2006.

Kanakidou, M., Seinfeld, J. H., Pandis, S. N., Barnes, I., Dentener, F. J., Facchini, M. C., Van Dingenen, R., Ervens, B., Nenes, A., Nielsen, C. J., Swietlicki, E., Putaud, J. P., Balkanski, Y., Fuzzi, S., Horth, J., Moortgat, G. K., Winterhalter, R., Myhre, C. E. L., Tsigaridis, K., Vignati, E., Stephanou, E. G., and Wilson, J.: Organic aerosol and global climate modelling: a review, Atmos. Chem. Phys., 5, 1053-1123, 2005.

Karl, M., Tsigaridis, K., Vignati, E., and Dentener, F.: Formation of secondary organic aerosol from isoprene oxidation over Europe, Atmos. Chem. Phys., 9, 7003-7030, 2009.

Kerkweg, A., Sander, R., Tost, H., and Jöckel, P.: Technical note: Implementation of prescribed (OFFLEM), calculated (ONLEM), and pseudo-emissions (TNUDGE) of chemical species in the Modular Earth Submodel System (MESSy), Atmos. Chem. Phys., 6, 3603-3609, 10.5194/acp-6-3603-2006, 2006a.

Kerkweg, A., Buchholz, J., Ganzeveld, L., Pozzer, A., Tost, H., and Jöckel, P.: Technical Note: An implementation of the dry removal processes DRY DEPosition and SEDImentation in the Modular Earth Submodel System (MESSy), Atmos. Chem. Phys., 6, 4617-4632, 2006b.

Kodros, J. K., Papanastasiou, D. K., Paglione, M., Masiol, M., Squizzato, S., Florou, K., Skyllakou, K., Kaltsonoudis, C., Nenes, A., and Pandis, S. N.: Rapid dark aging of biomass burning as an overlooked source of oxidized organic aerosol, Proceedings of the National Academy of Sciences of the United States of America, 117, 33028-33033, 10.1073/pnas.2010365117, 2020.

Lambe, A. T., Onasch, T. B., Massoli, P., Croasdale, D. R., Wright, J. P., Ahern, A. T., Williams, L. R., Worsnop, D. R., Brune, W. H., and Davidovits, P.: Laboratory studies of the chemical composition and cloud condensation nuclei (CCN) activity of secondary organic aerosol (SOA) and oxidized primary organic aerosol (OPOA), Atmospheric Chemistry and Physics, 11, 8913-8928, 10.5194/acp-11-8913-2011, 2011.

Lauer, A., Eyring, V., Hendricks, J., Joeckel, P., and Lohmann, U.: Global model simulations of the impact of ocean-going ships on aerosols, clouds, and the radiation budget, Atmos. Chem. Phys., 7, 5061-5079, 2007.

Liu, L., ; Thorsten Hohaus; Philipp Franke; Anne C. Lange; Ralf Tillmann; Hendrik Fuchs; Zhaofeng Tan; Franz Rohrer; Vlassis Karydis; Quanfu He; Vaishali Vardhan; Stefanie Andres; Birger Bohn; Frank Holland; Benjamin Winter; Sergej Wedel; Anna Novelli; Andreas Hofzumahaus; Andreas Wahner; and Astrid Kiendler-Scharr: Observational evidence reveals the significance of nocturnal chemistry in secondary organic aerosol formation across all seasons, npj Climate and Atmospheric Science, in review, 2024.

MESSy Consortium: The Modular Earth Submodel System (Version 2.55.2_1027-oracle-lite_de2c6f2b), Zenodo [code], https://zenodo.org/records/19204803, 2026.

Mortier, A., Gliß, J., Schulz, M., Aas, W., Andrews, E., Bian, H., Chin, M., Ginoux, P., Hand, J., Holben, B., Zhang, H., Kipling, Z., Kirkevåg, A., Laj, P., Lurton, T., Myhre, G., Neubauer, D., Olivié, D., von Salzen, K., Skeie, R. B., Takemura, T., and Tilmes, S.: Evaluation of climate model aerosol trends with ground-based observations over the last 2 decades – an AeroCom and CMIP6 analysis, Atmos. Chem. Phys., 20, 13355-13378, 10.5194/acp-20-13355-2020, 2020.

Murphy, B. N., Donahue, N. M., Fountoukis, C., and Pandis, S. N.: Simulating the oxygen content of ambient organic aerosol with the 2D volatility basis set, Atmos. Chem. Phys., 11, 7859-7873, 2011.

Murphy, B. N., Donahue, N. M., Fountoukis, C., Dall'Osto, M., O'Dowd, C., Kiendler-Scharr, A., and Pandis, S. N.: Functionalization and fragmentation during ambient organic aerosol aging: application of the 2-D volatility basis set to field studies, Atmospheric Chemistry and Physics, 12, 10797-10816, 10.5194/acp-12-10797-2012, 2012.

Ng, N. L., Kroll, J. H., Keywood, M. D., Bahreini, R., Varutbangkul, V., Flagan, R. C., Seinfeld, J. H., Lee, A., and Goldstein, A. H.: Contribution of first- versus second-generation products to secondary organic aerosols formed in the oxidation of biogenic hydrocarbons, Environ. Sci. Technol., 40, 2283-2297, 2006.

https://doi.org/10.5194/egusphere-2026-1709
Preprint. Discussion started: 8 April 2026

Paglione, M., Gilardoni, S., Rinaldi, M., Decesari, S., Zanca, N., Sandrini, S., Giulianelli, L., Bacco, D., Ferrari, S., Poluzzi, V., Scotto, F., Trentini, A., Poulain, L., Herrmann, H., Wiedensohler, A., Canonaco, F., Prévôt, A. S. H., Massoli, P., Carbone, C., Facchini, M. C., and Fuzzi, S.: The impact of biomass burning and aqueous-phase processing on air quality: a multi-year source apportionment study in the Po Valley, Italy, Atmos. Chem. Phys., 20, 1233-1254, 10.5194/acp-20-1233-2020, 2020.

Pai, S. J., Heald, C. L., Pierce, J. R., Farina, S. C., Marais, E. A., Jimenez, J. L., Campuzano-Jost, P., Nault, B. A., Middlebrook, A. M., Coe, H., Shilling, J. E., Bahreini, R., Dingle, J. H., and Vu, K.: An evaluation of global organic aerosol schemes using airborne observations, Atmos. Chem. Phys., 20, 2637-2665, 10.5194/acp-20-2637-2020, 2020.

Pandis, S. N., Wexler, A. S., and Seinfeld, J. H.: Secondary organic aerosol formation and transport. 2. Predicting the ambient secondary organic aerosol-size distribution, Atmos. Environ. A-Gen., 27, 2403-2416, 1993.

Pathak, R. K., Presto, A. A., Lane, T. E., Stanier, C. O., Donahue, N. M., and Pandis, S. N.: Ozonolysis of alpha-pinene: parameterization of secondary organic aerosol mass fraction, Atmospheric Chemistry and Physics, 7, 3811-3821, 2007.

Peñuelas, J. and Staudt, M.: BVOCs and global change, Trends in Plant Science, 15, 133-144, 10.1016/j.tplants.2009.12.005, 2010.

Pozzer, A., Reifenberg, S. F., Kumar, V., Franco, B., Kohl, M., Taraborrelli, D., Gromov, S., Ehrhart, S., Jöckel, P., Sander, R., Fall, V., Rosanka, S., Karydis, V., Akritidis, D., Emmerichs, T., Crippa, M., Guizzardi, D., Kaiser, J. W., Clarisse, L., Kiendler-Scharr, A., Tost, H., and Tsimpidi, A.: Simulation of organics in the atmosphere: evaluation of EMACv2.54 with the Mainz Organic Mechanism (MOM) coupled to the ORACLE (v1.0) submodel, Geoscientific Model Development, 15, 2673-2710, 10.5194/gmd-15-2673-2022, 2022.

Pringle, K. J., Tost, H., Message, S., Steil, B., Giannadaki, D., Nenes, A., Fountoukis, C., Stier, P., Vignati, E., and Leieved, J.: Description and evaluation of GMXe: a new aerosol submodel for global simulations (v1), Geoscientific Model Development, 3, 391-412, 2010.

Pugh, T. A. M., MacKenzie, A. R., Hewitt, C. N., Langford, B., Edwards, P. M., Furneaux, K. L., Heard, D. E., Hopkins, J. R., Jones, C. E., Karunaharan, A., Lee, J., Mills, G., Misztal, P., Moller, S., Monks, P. S., and Whalley, L. K.: Simulating atmospheric composition over a South-East Asian tropical rainforest: performance of a chemistry box model, Atmos. Chem. Phys., 10, 279-298, 2010.

Pye, H. O. T., D'Ambro, E. L., Lee, B., Schobesberger, S., Takeuchi, M., Zhao, Y., Lopez-Hilfiker, F., Liu, J. M., Shilling, J. E., Xing, J., Mathur, R., Middlebrook, A. M., Liao, J., Welti, A., Graus, M., Warneke, C., de Gouw, J. A., Holloway, J. S., Ryerson, T. B., Pollack, I. B., and Thornton, J. A.: Anthropogenic enhancements to production of highly oxygenated molecules from autoxidation, Proceedings of the National Academy of Sciences of the United States of America, 116, 6641-6646, 10.1073/pnas.1810774116, 2019.

Riipinen, I., Talvinen, S., Chassaing, A., Georgakaki, P., Li, X., García-Pando, C. P., Bergman, T., Kommula, S. M., Proske, U., Gkouvousis, A., Tsimpidi, A. P., Chatziparaschos, M., Neuberger, A., Karydis, V. A., Calderón, S. M., Romakkaniemi, S., Partridge, D. G., Khadir, T., Dada, L., van Noije, T., Decesari, S., Seland, Ø., Zieger, P., Bender, F., Carslaw, K., Cermak, J., Costa-Surós, M., Gonçalves Ageitos, M., Gramlich, Y., Haugvaldstad, O. W., Holopainen, E., Hoose, C., Jorba, O., Kakavas, S., Kanakidou, M., Kokkola, H., Krejci, R., Kühn, T., Kulmala, M., Le Sager, P., Makkonen, R., Manavi, S. E. I., Mentel, T. F., Milousis, A., Myriokefalitakis, S., Nenes, A., Nieminen, T., Pandis, S. N., Patoulias, D., Petäjä, T., Quaas, J., Regayre, L., Scholz, S. M. C., Schulz, M., Skyllakou, K., Sousse, R., Stier, P., Thomas, M. A., Villinger, J. T., Virtanen, A., Wyser, K., and Ekman, A. M. L.: Treatment of Key Aerosol and Cloud Processes in Earth System Models – Recommendations from the FORCeS Project, Tellus B: Chemical and Physical Meteorology, 10.16993/tellusb.1883, 2026.

Röckner, E., Brokopf, R., Esch, M., Giorgetta, M., Hagemann, S., Kornblueh, L., Manzini, E., Schlese, U., and Schulzweida, U.: Sensitivity of simulated climate to horizontal and vertical resolution in the ECHAM5 atmosphere model, J. Climate, 19, 3771-3791, 2006.

https://doi.org/10.5194/egusphere-2026-1709
Preprint. Discussion started: 8 April 2026

Roeckner, E., Brokopf, R., Esch, M., Giorgetta, M., Hagemann, S., Kornblueh, L., Manzini, E., Schlese, U., and Schulzweida, U.: Sensitivity of simulated climate to horizontal and vertical resolution in the ECHAM5 atmosphere model, Journal of Climate, 19, 3771-3791, 10.1175/jcli3824.1, 2006.

Sander, R., Baumgaertner, A., Cabrera-Perez, D., Frank, F., Gromov, S., Grooss, J. U., Harder, H., Huijnen, V., Jockel, P., Karydis, V. A., Niemeyer, K. E., Pozzer, A., Hella, R. B., Schultz, M. G., Taraborrelli, D., and Tauer, S.: The community atmospheric chemistry box model CAABA/MECCA-4.0, Geoscientific Model Development, 12, 1365-1385, 10.5194/gmd-12-1365-2019, 2019.

Scholz, S. M. C., Karydis, V. A., Gkatzelis, G. I., Fuchs, H., Pandis, S. N., and Tsimpidi, A. P.: Incorporation of lumped IVOC emissions into the ORACLE model (V1.1): a multi-product framework for assessing global SOA formation from internal combustion engines, Geosci. Model Dev., 18, 10119-10142, 10.5194/gmd-18-10119-2025, 2025.

Seco, R., Peñuelas, J., Filella, I., Llusià, J., Molowny-Horas, R., Schallhart, S., Metzger, A., Müller, M., and Hansel, A.: Contrasting winter and summer VOC mixing ratios at a forest site in the Western Mediterranean Basin: the effect of local biogenic emissions, Atmos. Chem. Phys., 11, 13161-13179, 10.5194/acp-11-13161-2011, 2011.

Shrivastava, M., Cappa, C. D., Fan, J. W., Goldstein, A. H., Guenther, A. B., Jimenez, J. L., Kuang, C., Laskin, A., Martin, S. T., Ng, N. L., Petaja, T., Pierce, J. R., Rasch, P. J., Roldin, P., Seinfeld, J. H., Shilling, J., Smith, J. N., Thornton, J. A., Volkamer, R., Wang, J., Worsnop, D. R., Zaveri, R. A., Zelenyuk, A., and Zhang, Q.: Recent advances in understanding secondary organic aerosol: Implications for global climate forcing, Reviews of Geophysics, 55, 509-559, 10.1002/2016rg000540, 2017.

Spracklen, D. V., Jimenez, J. L., Carslaw, K. S., Worsnop, D. R., Evans, M. J., Mann, G. W., Zhang, Q., Canagaratna, M. R., Allan, J., Coe, H., McFiggans, G., Rap, A., and Forster, P.: Aerosol mass spectrometer constraint on the global secondary organic aerosol budget, Atmospheric Chemistry and Physics, 11, 12109-12136, 10.5194/acp-11-12109-2011, 2011.

Strader, R., Lurmann, F., and Pandis, S. N.: Evaluation of secondary organic aerosol formation in winter, Atmos. Environ., 33, 4849-4863, 1999.

Tost, H., Jockel, P. J., Kerkweg, A., Sander, R., and Lelieveld, J.: Technical note: A new comprehensive SCAVenging submodel for global atmospheric chemistry modelling, Atmos. Chem. Phys., 6, 565-574, 2006.

Tsigaridis, K., Daskalakis, N., Kanakidou, M., Adams, P. J., Artaxo, P., Bahadur, R., Balkanski, Y., Bauer, S. E., Bellouin, N., Benedetti, A., Bergman, T., Berntsen, T. K., Beukes, J. P., Bian, H., Carslaw, K. S., Chin, M., Curci, G., Diehl, T., Easter, R. C., Ghan, S. J., Gong, S. L., Hodzic, A., Hoyle, C. R., Iversen, T., Jathar, S., Jimenez, J. L., Kaiser, J. W., Kirkevag, A., Koch, D., Kokkola, H., Lee, Y. H., Lin, G., Liu, X., Luo, G., Ma, X., Mann, G. W., Mihalopoulos, N., Morcrette, J. J., Mueller, J. F., Myhre, G., Myriokefalitakis, S., Ng, N. L., O'Donnell, D., Penner, J. E., Pozzoli, L., Pringle, K. J., Russell, L. M., Schulz, M., Sciare, J., Seland, O., Shindell, D. T., Sillman, S., Skeie, R. B., Spracklen, D., Stavrakou, T., Steenrod, S. D., Takemura, T., Tiitta, P., Tilmes, S., Tost, H., van Noije, T., van Zyl, P. G., von Salzen, K., Yu, F., Wang, Z., Wang, Z., Zaveri, R. A., Zhang, H., Zhang, K., Zhang, Q., and Zhang, X.: The AeroCom evaluation and intercomparison of organic aerosol in global models, Atmospheric Chemistry and Physics, 14, 10845-10895, 10.5194/acp-14-10845-2014, 2014.

Tsimpidi, A. P., Karydis, V. A., and Pandis, S. N.: Response of Fine Particulate Matter to Emission Changes of Oxides of Nitrogen and-Anthropogenic Volatile Organic Compounds in the Eastern United States, J. Air Waste Manage. Assoc., 58, 1463-1473, 10.3155/1047-3289.58.11.1463, 2008.

Tsimpidi, A. P., Karydis, V. A., Pandis, S. N., and Lelieveld, J.: Global combustion sources of organic aerosols: model comparison with 84 AMS factor-analysis data sets, Atmos. Chem. Phys., 16, 8939-8962, 10.5194/acp-16-8939-2016, 2016.

Tsimpidi, A. P., Karydis, V. A., Pozzer, A., Pandis, S. N., and Lelieveld, J.: ORACLE (v1.0): module to simulate the organic aerosol composition and evolution in the atmosphere, Geoscientific Model Development, 7, 3153-3172, 10.5194/gmd-7-3153-2014, 2014.

https://doi.org/10.5194/egusphere-2026-1709
Preprint. Discussion started: 8 April 2026

Tsimpidi, A. P., Karydis, V. A., Pozzer, A., Pandis, S. N., and Lelieveld, J.: ORACLE 2-D (v2.0): an efficient module to compute the volatility and oxygen content of organic aerosol with a global chemistry-climate model, Geoscientific Model Development, 11, 3369-3389, 10.5194/gmd-11-3369-2018, 2018.

Tsimpidi, A. P., Scholz, S. M. C., Milousis, A., Mihalopoulos, N., and Karydis, V. A.: Aerosol composition trends during 2000-2020: in-depth insights from model predictions and multiple worldwide near-surface observation datasets, Atmospheric Chemistry and Physics, 25, 10183-10213, 10.5194/acp-25-10183-2025, 2025.

Tsimpidi, A. P., Karydis, V. A., Zavala, M., Lei, W., Bei, N., Molina, L., and Pandis, S. N.: Sources and production of organic aerosol in Mexico City: insights from the combination of a chemical transport model (PMCAMx-2008) and measurements during MILAGRO, Atmos. Chem. Phys., 11, 5153-5168, 2011.

Tsimpidi, A. P., Karydis, V. A., Zavala, M., Lei, W., Molina, L., Ulbrich, I. M., Jimenez, J. L., and Pandis, S. N.: Evaluation of the volatility basis-set approach for the simulation of organic aerosol formation in the Mexico City metropolitan area, Atmos. Chem. Phys., 10, 525-546, 2010.

van der Werf, G. R., Randerson, J. T., Giglio, L., van Leeuwen, T. T., Chen, Y., Rogers, B. M., Mu, M. Q., van Marle, M. J. E., Morton, D. C., Collatz, G. J., Yokelson, R. J., and Kasibhatla, P. S.: Global fire emissions estimates during 1997-2016, Earth System Science Data, 9, 697-720, 10.5194/essd-9-697-2017, 2017.

Xu, W., Han, T., Du, W., Wang, Q., Chen, C., Zhao, J., Zhang, Y., Li, J., Fu, P., Wang, Z., Worsnop, D. R., and Sun, Y.: Effects of Aqueous-Phase and Photochemical Processing on Secondary Organic Aerosol Formation and Evolution in Beijing, China, Environ Sci Technol, 51, 762-770, 10.1021/acs.est.6b04498, 2017.

Young, P. J., Archibald, A. T., Bowman, K. W., Lamarque, J. F., Naik, V., Stevenson, D. S., Tilmes, S., Voulgarakis, A., Wild, O., Bergmann, D., Cameron-Smith, P., Cionni, I., Collins, W. J., Dalsøren, S. B., Doherty, R. M., Eyring, V., Faluvegi, G., Horowitz, L. W., Josse, B., Lee, Y. H., MacKenzie, I. A., Nagashima, T., Plummer, D. A., Righi, M., Rumbold, S. T., Skeie, R. B., Shindell, D. T., Strode, S. A., Sudo, K., Szopa, S., and Zeng, G.: Pre-industrial to end 21st century projections of tropospheric ozone from the Atmospheric Chemistry and Climate Model Intercomparison Project (ACCMIP), Atmos. Chem. Phys., 13, 2063-2090, 10.5194/acp-13-2063-2013, 2013.